# Circulating extracellular vesicle-associated TGFβ3 modulates response to cytotoxic therapy in head and neck squamous cell carcinoma

Dorival Mendes Rodrigues-Junior[1,2], Ph.D., Soon Sim Tan[3], Sai Kiang Lim[3], Ph.D., Hui Sun Leong[2], Matias Eliseo Melendez[4], PhD., Cintia Regina Niederauer Ramos[4], Luciano de Souza Viana[4], M.D., PhD., Daniel SW Tan[2,5], M.D., Ph.D., Andre Lopes Carvalho[4], M.D., Ph.D., M.P.H., N. Gopalakrishna Iyer[2,6*], M.D., Ph.D., Andre Luiz Vettore[1*], Ph.D.

*[1]Department of Biological Sciences, Universidade Federal de São Paulo, Diadema, Brasil. [2]Cancer Therapeutics Research Laboratory, National Cancer Centre of Singapore, Singapore. [3]Istitute of Medical Biology, A*-STAR, Singapore. [4]Molecular Oncology Research Center, Barretos Cancer Hospital, Barretos, SP, Brazil. [5]Division of Medical Oncology, National Cancer Centre of Singapore, Singapore. [6]Division of Surgical Oncology, National Cancer Centre of Singapore, Singapore.*

*** Corresponding author:**
Andre L. Vettore, Ph.D., Laboratório de Biologia Molecular do Câncer, UNIFESP, Rua Pedro de Toledo, 669 – 11° andar, São Paulo, SP, Brazil, 04039-032. E-mail: andre.vettore@gmail.com

N. Gopalakrishna Iyer, MD, Ph.D., Cancer Therapeutics Research Laboratory, National Cancer Centre of Singapore. 11 Hospital Drive, Singapore, 169610. E-mail: gopaliyer@nccs.com.sg

**Financial support:** This study was supported by grants from National Cancer Centre Singapore Research Foundation (#NMRC/CSA-INV/011/2016) and Fundação de Amparo à Pesquisa do Estado de São Paulo – FAPESP (#2015/09182-0)

## Abstract

Management of locally-advanced head and neck squamous cell carcinoma (HNSCC) requires a multi-prong approach comprising surgery, radiation- and/or chemo-therapy, yet outcomes are limited. This is largely due to a paucity of biomarkers that can predict response to specific treatment modalities. Here, we evaluated TGFβ3 protein levels in extracellular vesicles (EV) released by HNSCC cells as a predictor for response to chemoradiation therapy (CRT). To this end, specific EV-fractions were isolated from cell lines or HNSCC patient plasma, and TGFβ3 protein was quantified. In patients treated with CRT, TGFβ3 levels were found to be significantly higher in plasma EV-fractions or non-responders compared to responders. High levels of TGFβ3 levels in Annexin V-EVs were associated with the worst progression-free survival. *In vitro* experiments demonstrated that TGFβ3-silencing sensitized HNSCC cells to cytotoxic therapies, and this phenotyped could be rescued by treatment with exogenous. In addition, specific EV-fractions shed by cisplatin-resistant cells were sufficient to transfer the resistant phenotype to sensitive cells through activation of TGFβ-signaling pathway. Therefore, our data show that TGFβ3 transmitted through EV plays a significant role in response to cytotoxic therapy, which can be exploited as a potential biomarker for CRT response in HNSCC-patients treated with curative intent.


**Key words:** Head and Neck Cancer, Chemoradiation therapy, Treatment Response, Extracellular Vesicles, Exosomes, Microvesicles, TGFβ, Plasma biomarker.

## Introduction

Biomarker-directed therapeutic decisions remain the cornerstone for precision oncology, most widely practiced in the utilization of targeted therapy. However, it is equally critical to define biomarkers of response to conventional cytotoxic therapy, commonly used for most solid tumors. This is evident in head and neck squamous cell carcinoma (HNSCC), which is one of the commonest lethal malignancies worldwide (1,2). For locally advanced HNSCC affecting the oropharynx, larynx, and hypopharynx, concurrent chemoradiation therapy (CRT), with or without induction chemotherapy (IC) has been established as the paradigm of treatment with curative intent (3). Nonetheless, a significant number of patients fail to respond and develop recurrent/progressive disease, where surgery is the only available option. For these patients, ineffective treatment choices result in an unwanted delay of potentially curative surgery. In addition, surgery is made challenging in a heavily pre-treated patient and a radiated field (4). The ability to predict treatment-failure and identify patients early could help to optimize treatment decisions and direct patients to more aggressive treatment up-front. Therefore, there is an unmet need for robust, and ideally non-invasive predictive biomarkers for HNSCC treated with CRT.

In this context, non-invasive, robust blood-based markers are ideal, and if these can be shown to be involved in the biology of treatment response also have the additional potential to be therapeutic targets (5). However, identifying putative markers in the blood, plasma or serum is fraught with many technical issues, especially the presence of high-abundance proteins in these compartments, resulting in low signal-to-noise ratio. The discovery of extracellular vesicles (EVs: exosomes, microvesicles, apoptotic bodies) could circumvent these issues and allow analyses of a much ‘cleaner’ serum/plasma compartments (6).

EVs are lipid bilayer membrane vesicles carrying proteins, lipids, nucleic acids, and sugars (6,7). Tumor cells are avid EV producers, which can function in a paracrine manner or carried through the circulation to target cells (8,9), where their cargo can influence immune evasion, tumorigenesis, cancer progression, metastatic spread and response to treatment (10-12). Of note, HNSCC are known to produce EVs into the circulation (13,14). These could potentially be used in diagnosis, prognosis and predicting response to treatment, as they offer a non-invasive window into the tumor and its microenvironment (15). In particular, EVs have been implicated in mediating drug resistance in tumor cells by transferring proteins such as P-glycoprotein (ABCB1) able to export drugs or sequester drugs in EVs for removal from tumor cells or transferring miRNA to activate genes to counter the effects of the drugs in recipient cells (11).

We recently conducted a high-throughput screen of specific plasma EVs, comparing responders and non-responders in HNSCC treated with CRT to identify potential markers of treatment-response (16). Among the potential markers in plasma EVs, TGFβ3 emerged as a putative candidate that correlated with treatment. Previous studies have shown that transforming growth factor beta (TGFβ) signaling appears to have a widespread function in tumor initiation, progression, and metastases (17-19). TGFβ superfamily has also been implicated in epithelial-mesenchymal transition and maintaining the stem cell fraction, which in turn plays an important role in radio- and chemo-resistance. Consistent with this, TGFβ1 expression in HNSCCs has been shown to correlate with poor disease outcome, but not with treatment response (20,21). Although plasma levels of TGFβ have been used as a prognostic marker in gastric, breast, lung, hepatocellular, colorectal, and renal cell carcinomas (22-27), its use in HNSCC, especially in the context of treatment response remains untested.

Based on our previous screen, we, therefore, examined the association of circulating EV-associated TGFβ3 with resistance to cytotoxic chemo- and radiation therapy in HNSCC. Our data demonstrate the potential of TGFβ3 in circulating extracellular vesicles as a potential blood-based predictive biomarker for treatment response in HNSCC patients treated with chemoradiation therapy and suggests a role for EV-TGFβ3 signaling in mediating resistance to cytotoxic drugs.

## Material and Methods

### Patients and trial

This study involved plasma samples from 38 patients with locally advanced HNSCC who underwent chemoradiotherapy protocol as part of a phase 2 clinical trial to test the effect of IC followed by concomitant CRT in the treatment of HNSCC patients between 2009 and 2010 at the Department of Head and Neck Surgery, Barretos Cancer Hospital (Barretos, SP, Brazil). In summary, IC consisted of intravenous paclitaxel (175 mg/m$^2$) and cisplatin (80 mg/m$^2$), and CRT consisted of concomitant radiotherapy (2 Gy/day, 5 days/week for 7 weeks) and cisplatin (100 mg/m$^2$, administered intravenous on days 1, 22, and 43), initiated at 3 weeks after the third cycle of IC (4).

This study was approved by the ethics committees of Federal University of São Paulo (#1610/2016) and Barretos Cancer Hospital (#231/2009). The study included patients with histologically confirmed locally advanced stage III or IV a-b (M0) squamous cell carcinoma of the oral cavity, larynx, oropharynx, or hypopharynx, that signed an informed consent to undergo the treatment as outlined. All patients were required to have measurable disease by Response Evaluation Criteria in Solid Tumors (RECIST, version 1.1) at the start point, and disease response was evaluated after IC and after CRT using the RECIST criteria. Briefly, tumor response to treatment was

considered as complete response (CR) when there was the disappearance of all detectable lesions, and non-response (NR) as tumor response less than complete, the appearance of a new lesion, or increase of any lesion classified as measurable at initial examination (including tumor recurrence). Further details of the trial, including the definition of tumor response as partial response (PR), stable disease (SD) or progression of disease (PD) can be found in the previously published results (4). For statistical analysis, patients with CR and PR after IC were grouped and compared to those with SD or PD. On the other hand, when considering CRT response, only patients with CR were compared with all NR patients, which included those presenting PR, SD or PD after the completion of the treatment protocol. All plasma samples were collected at diagnosis, before chemoradiation therapy (pre-treatment samples).

**Cell line culture and treatment**

HNSCC cell lines used in this study were either obtained from ATCC (FaDu-ATCC HTB-43 and SCC25-ATCC CRL-1628) or patient-derived (NCC-HN120 and NCC-HN137). The cisplatin-resistant (CisR) lines used in this study were previously described (28,29). The authenticity of the commercial cell lines was confirmed by short tandem repeat STR profiling method and carried out 6 months before the start of the experiments. For drug treatment, control cells (CTRL) were treated with 10μM of TGFβR inhibitor (TGFβRi; #LY2109761, Cayman Chemical, Michigan, USA) and the cells$^{-TGFβ3}$ with 10ng/mL of exogenous TGFβ3 (#PT-4124, Lonza, Basel, Switzerland). Subsequent cytotoxic drug doses were as follows for SCC25 and FaDu cells: 5.0μM and 10μM of cisplatin (#PHR1624; Sigma Aldrich, St Louis, USA) or 0.01μM and 0.03μM of paclitaxel (#PHR1803; Sigma Aldrich, St Louis, USA), respectively. Proliferation was quantified using MTS assays (CellTiter-Glo, Promega, Madison, USA) according

to the manufacturer's protocol. The relative luminescence units from treated wells were normalized against DMSO control wells and expressed as a percentage of viable cells. Apoptosis was quantified using Annexin V-FITC assays according to the manufacturer's protocol (#1006; Biovision, San Francisco, USA). All treatment experiments were performed in triplicate, with three separate biological replicates for each assay.

For cell lines EVs-based treatment, cisplatin-sensitive cells were incubated for 72 hours with cisplatin (1.0µM) or paclitaxel (0.01nM) in EV-Free media, that consists of RPMI-1640 (ThermoFisher, Waltham, USA) supplemented with 10% fetal bovine serum (ThermoFisher, Waltham, USA) and 0.01 µg/mL of penicillin-streptomycin (ThermoFisher, Waltham, USA) filtered in a 50 kDa Ultra-15 Centrifugal Filter (Amicon; Millipore, Massachusetts, USA), with or without the addition of the Vesicular Secretome Fraction (VSF; volume normalized to the equivalent to 100ng of CD81) previously harvested from CisR cells. After this co-treatment, functional assays were performed to observe if EVs could mediate cisplatin response.

**EVs isolation**

To isolate EVs, the cells were incubated for 72 hours in phenol-red free DMEM (#31053, Gibco, Waltham, USA), supplemented with 5% Insulin-Transferrin-Selenium-Ethanolamine (#51500-056, ThermoFisher, Waltham, USA), 10mM of Non Essential Amino Acids (#11140-050, ThermoFisher, Waltham, USA), 500µg of fibroblast growth factor-basic (#13256-029, ThermoFisher, Waltham, USA), 100mM of Sodium Pyruvate and 55mM of β-Mercaptoethanol (#21985-023, ThermoFisher, Waltham, USA). After 72 hours, the culture medium was collected and centrifuged at 250 x *g* for 5 minutes to remove the dead cells. The supernatant was filtered on a 0.22µm filter and further

concentrated 20X by tangential flow filtration on a 50kDa Ultra-15 Centrifugal Filter (Amicon; Millipore, Massachusetts, USA) by centrifugation at 1200 x *g* for 20 minutes. This concentrated fraction is the Vesicular Secretome Fraction (VSF).

EVs fractions could be differentiated by their membrane phospholipid composition: specifically GM1-gangliosides and phosphatidylserine, which have a high specific binding affinity for *Cholerae* Toxin chain B (CTB) and Annexin V (AV), respectively (30,31). Briefly, 150µl of plasma or 100µl of VSF were incubated with 0.5µg of biotinylated CTB (#C34779; ThermoFisher, Waltham, USA) or 0.5µg of biotinylated AV (#K109, Biovision, San Francisco, USA) in 100µl of PBS or AV binding buffer, respectively for 60 minutes at 37°C. After the addition of 50µl of pre-washed Dynabeads MyOne Streptavidin T1 (#65602; ThermoFisher, Waltham, USA), the mixture was incubated for 30 minutes at 25°C. The magnetic beads were immobilized and the supernatant was collected as EV-depleted fraction. The beads were washed three times with 200µL of PBS and the isolated EVs bounded to CTB or AV-beads were stored at -20°C for up to 30 days.

**Characterization of EVs**

The size distribution of EVs present in the VSF was measured using the ZetaView (Particle Metrix, Ammersee, Germany) or NanoSight (Malvern, Worcestershire, UK). The modal diameter of the EVs was used in the statistical analyses. To visualize EVs through scanning electron microscopy, the VSF preparation was incubated with biotinylated CTB or AV and CTB-/AV-bound EVs were captured on streptavidin-coated polystyrene particles (#SVP-15-5; Spherotec, Chicago, USA), as previously described (31). The beads were suspended in 50µl of PBS and fixed with formaldehyde solution (formaldehyde 2%, glutaraldehyde 2.5%, sodium cacodylate

0.1M pH 7.2) before scanning on a FEI Quanta 250 FEG scanning electron microscope (ThermoFisher, Waltham, USA).

**ELISA**

Enzyme-Linked Immunosorbent Assay (ELISA) was used to quantify CD81 and TGFβ3 in CTB- or AV-EV fraction present in VSF or plasma samples. For CD81 detection, after EVs extraction, immobilized beads were washed twice with 100 µL wash buffer (0.1% BSA in PBS) and incubated with 100 µL of 1:500 diluted anti-CD81 antibodies (#SC-7637; Santa Cruz Biotechnologies, Dallas, USA), washed and incubated again with 1:5,000 diluted HRP-conjugated goat anti-mouse secondary antibodies 1:5,000 diluted (#SC-2031; Santa Cruz Biotechnologies, Dallas, USA). HRP activity was determined using Amplex Red Substrate (Life Technology, Grand Island, NY) as per manufacturer's protocol. The relative levels of CD81 in CTB- or AV-EVs were established as the ratio of the number of total cells (x) per total protein amount that was measured when the VSF was collected (y), by the respective concentration of CD81 (z) [(x/y)/z]. For TGFβ3 uncovering, CTB- and AV-EVs isolated were lysed with cell lysis buffer (#K269; Biovision) and ELISA sandwich assay was conducted following the manufacturer's instructions (#LS-F2825; LSBio, Seattle, Washington, USA), in which the EVs content and crude plasma were previously incubated with solution A (1N HCl) and B (1.2N NaOH/ 0.5M HEPES) for TGFβ3 activation. The CD81 expression level normalized the relative expression level of TGFβ3 (pg/mL) in EVs shed by cell lines.

**RNA extraction, cDNA synthesis and RT-PCR**

RNA extraction and RT-qPCR were performed as previously described (32). Expression levels of the three isoforms of TGFβ were determined by RT-PCR using *beta-actin* (*ACTB*) levels to normalize expression. The primer sequences for *TGFβ* isoforms were previously described (33).

**Knock out - CRISPR-Cas9 system**

pSpCas9(BB)-2A-Puro (pX459) V2.0 plasmid was used as a delivery system (34). gRNA sequences targeting *TGFβ3* and a scramble gRNA (**Supplementary Table 1**) were cloned at BbsI restriction site of pX459 plasmid. After sequencing validation, transfections were performed by electroporation using a Nucleofector 2b following the manufacturer's recommendations (Cell Line Nucleofector Kit C, program X-005; Lonza, Basel, Switzerland) with 2.0µg of pX459-gRNA plasmids and $1x10^6$ cells. Cells transfected with scramble CTRL and cells $^{-TGFβ3}$ (TGFβ3 knocked-out) were selected with puromycin (FaDu 2.5µM and SCC25 1.0µM). The TGFβ3 knockout was confirmed by Western blot.

**Western blot**

Western blots were performed as previously described (29). Antibodies used were purchased from Cell Signaling (Massachusetts, USA): anti-SMAD2 (#5339), anti-pSMAD2 (#18338), anti-ERK (#4695), anti-pERK (#4370), anti-αβTUBULIN (#2148), anti-GAPDH (#8884), goat anti-mouse (#7076), anti-rabbit IgG HRP-linked (#7074), or from Santa Cruz Biotechnology (Dallas, USA): anti-TGFβ3 (#166833), anti-CD9 (#SC-

13118), and anti-CD81 (#SC-7637). ImageJ bundled with Java 1.8.0_172 (U. S. National Institutes of Health, Maryland, USA) was used to normalize TGFβ3 intensity, according to αβ-TUBULIN expression.

**Statistical analyses**

Comparison of values obtained in cell viability and cell death assays were analyzed with GraphPad Prism 6 (GraphPad Software Inc., San Diego, USA) using one-way ANOVA and multiple paired comparisons were conducted by means of the Bonferroni's post-test method.

Mann-Whitney, $\chi^2$ or Fisher exact tests were used to evaluate the associations between TGFβ3 expression, treatment response, disease progression and clinical variables, as appropriate. The Kaplan–Meier method was used to estimate the progression-free survival (PFS) of patients, and the log-rank test was used to examine the differences between groups. A multivariate logistic regression was performed to identify the independent variables associated with treatment response in the organ preservation protocol and performed in a step-forward fashion to estimate the odds ratio (OR). The multivariate logistic regression model included clinical and molecular variables with p-value < 0.20 in the univariate analysis to build a final model. The final model was further adjusted for clinically relevant variables. These statistical analyses were performed using SPSS statistics 23.0 (IBM, New York, USA). A p-value<0.05 was necessary to determine all statistically significant differences.

## Results

### Plasma TGFβ3 expression correlates with disease progression

We had previously identified TGFβ3 as a potential marker for response to CRT in a high-throughput screen designed to compare plasma EV fractions between responders and non-responders to CRT. To validate these findings, we set out to quantify TGFβ3 protein levels in three distinct plasma compartments of patients treated with CRT: crude plasma, CTB-EVs, and AV-EVs. The clinical and histological features of the 38 patients with locally advanced HNSCC enrolled in this study are presented in **Supplementary Table 2**. In summary, the median follow-up for this cohort was 4 years and the patients were predominantly males (n = 34; 89.5%), with age ranging from 37 to 76 years (median: 56 years). The use of tobacco (current and former) was reported by 36 patients (94.8%), while only 5.3% of the cases were HPV-associated cancers. Primary tumor sites included oral cavity (n=2, 5.3%), oropharynx (n=22, 57.9%), hypopharynx (n=5, 13.2%) and larynx (n=9, 23.7%). Majority of tumors were locally advanced (T3/T4, 92.1%), and during the follow-up period 27 patients (71.1%) demonstrated complete response (CR) or partial response (PR) to induction chemotherapy and 22 patients (57.9%) presented complete response to CRT (there was 3 patients did not complete the treatment protocol, thus were not evaluated after the CRT).

TGFβ3 concentration was measured in CTB-EVs, AV-EVs and in crude plasma samples from blood obtained from patients prior to any treatment, and quantified using ELISA. TGFβ3 levels in CTB-EVs and AV-EVs had mean and median concentrations of 580.0 and 562.7 pg/mL (range: 73.1-1328 pg/mL), and 666.6 and 672.3 pg/mL

(range: 89.9 and 1390 pg/mL), respectively. In the total plasma samples, TGFβ3 concentration was significantly lower with mean and median of 13.9 and 5.6 pg/mL (range: 0-73.7 pg/mL). Importantly, TGFβ3 concentrations was significantly higher in CTB-EV and AV-EV fractions from non-responders compared to complete responders for both IC and CRT treatments (**Figure 1A** and **B**). In contrast, crude plasma concentration of TGFβ3 was not associated with treatment response. Based on the Youden index obtained from Receiver Operating Characteristic curves for IC response, cutoff values for TGFβ3 concentration in AV-EVs and CTB-EVs were 769.0 pg/mL (Area Under the ROC Curve; AUC: 0.912) and 585.0 pg/mL (AUC: 0.838), respectively (**Supplementary Figure 1**). These cutoff values were used to categorize patients and determine associations with clinical-pathological characteristics including age, gender, tobacco consumption, primary tumor site, HPV-status, resectability status, stage, and final response to CRT. Statistical analysis shows TGFβ3 concentration in AV-EVs was significantly associated with CRT response (**Table 1**). No other associations were observed between the other clinical features and concentration of TGFβ3. In line with this, Kaplan-Meier analysis for progression-free survival showed that patients with higher TGFβ3 levels in AV-EVs had poorer outcomes (**Figure 1C**). Based on the cutoff defined above, 73.3% of patients with high TGFβ3 levels in AV-EVs developed disease progression in four years, compared to 52.2% of patients with low TGFβ3 levels (p=0.038). Furthermore, logistic regression analysis adjusted by age, tumor resectability and TGFβ3 levels in plasma AV-EVs showed that TGFβ3 concentration (OR=9.14; 95%CI 1.50–55.50; p=0.016) and tumor resectability (OR=8.67; 95%CI 1.34–54.84; p=0.021) remained independent prognostic factors for final response to CRT (**Table 2**).

### *TGFβ3* expression in HNSCC cell lines

$IC_{50}$ levels for cisplatin were determined in two intrinsically resistant lines and in two pairs of isogenic patient-derived lines, where cisplatin resistance was established by stepwise increments of sub-lethal cisplatin doses. $IC_{50}$ levels for cisplatin resistant lines were: 36.3μM for NCC-HN120 CisR, 13.8μM for FaDu, 10.0μM for NCC-HN137 CisR, and 6.8μM for SCC25, while $IC_{50}$ levels for sensitive lines were: 2.8μM for NCC-HN120 and 1.0μM for NCC-HN137 (**Figure 2A** and **Supplementary Figure 2**). RT-qPCR assay was then performed to determine if the expression levels of *TGFβ* correlate with cisplatin sensitivity in these cell lines. We were not able to detect any correlation between cisplatin sensitivity and expression levels of *TGFβ1* or *TGFβ2* isoforms (**Figure 2B** and **2C**). However, the *TGFβ3* expression levels were higher in all four cisplatin resistant cell lines compared to sensitive lines (**Figure 2D**).

### TGFβ3 knockout sensitizes HNSCC cells to cytotoxic therapy

The CRISPR-Cas9 system was used to knockout TGFβ3 expression in FaDu and SCC25 cell lines to generate SCC25$^{-TGFβ3}$ and FaDu$^{-TGFβ3}$ cells. Compared to parental cells (FaDu WT and SCC25 WT) and knockout-scramble control lines (SCC25 CTRL and FaDu CTRL) both knockout cell lines showed dramatic reduction in TGFβ3 expression (reduced by 89.2 % for SCC25$^{-TGFβ3}$ and 95.7 % for FaDu$^{-TGFβ3}$) (**Figure 3A**). These were subject to drug treatment with either cisplatin or paclitaxel alone, or in the presence of exogenous TGFβ3 in the knockout cells or TGFβ receptor II-inhibitor (TGFβRi) in the CTRL cells. As predicted, SCC25$^{-TGFβ3}$ and FaDu$^{-TGFβ3}$ showed increased drug sensitivity, which was reversed by treatment with exogenous TGFβ3 (**Figure 3B** and **C**). In contrast, abrogating TGFβRII using the TGFβRi increased sensitivity to both cytotoxic drugs in SCC25 and FaDu CTRL cells. Similar results were

observed when drug effect was evaluated by measuring apoptosis using Annexin V staining assays (**Figure 3D** and **E**). These results support the clinical observation that manipulating TGFβ3 levels is necessary and sufficient to modulate the HNSCC response to cytotoxic therapies.

**Secretion and intercellular transfer of TGFβ3-containing EVs by cisplatin-resistant cells**

To determine whether HNSCC cell lines secrete TGFβ3 in EVs, culture media conditioned by NCC-HN120 WT and NCC-HN120 CisR were enriched for EVs by filtration. The enriched vesicular secretome fraction (VSF) was analyzed by ZetaView for the presence of nanoparticles. Both WT and CisR VSFs were enriched in nanoparticles with a mean size of 127.1 ± 1.51 nm for WT and 125.9 ± 1.21 nm for CisR (**Supplementary Figure 3A**). The VSFs were analyzed for the presence of lipid membrane entities by determining if some of the nanoparticles could be extracted by membrane lipid ligands such as CTB or AV. Briefly, the VSF from NCC-HN120 WT were incubated with biotinylated CTB or AV and then with streptavidin-conjugated polystyrene or magnetic beads to immobilize any CTB-EV or AV-EV. The beads were then visualized by scanning electron microscopy and were observed to bind vesicles-like nanoparticles of 100-200 nm consistent with the size range of lipid membrane nanoparticles estimated by ZetaView (**Supplementary Figure 3B**). To further confirm that these lipid membrane nanoparticles were EVs, we assayed CTB- and AV-EVs for the presence of CD81, a tetraspanin membrane protein commonly associated with EVs, by ELISA (**Supplementary Figure 3C**). CD81 was present on both CTB- and AV-EVs secreted by WT and CisR cell lines. Furthermore, the VSF collected from $SCC25^{-TGF\beta3}$ was analyzed by NanoSight, and the size distribution of the nanoparticles detected had a mean size of 96.46 ± 5.70 nm (**Supplementary Figure 4A**). The CD9 and CD81

expression was also observed SCC25$^{-TGF\beta3}$ by WB (**Supplementary Figure 4B**). Together, these observations confirmed that the VSFs have bona fide 50-200 nm EVs i.e. nano-size particles with membrane lipids and membrane proteins i.e. EVs.

Next, CTB- and AV-EVs were analyzed for the presence of TGFβ3 by the same ELISA assay used in plasma samples above. TGFβ3 protein levels were significantly higher in both CTB- and AV-EV fractions secreted by NCC-HN120 CisR cells compared to those by cisplatin-sensitive NCC-HN120 WT cells (**Figure 4A** and **B**). To determine if EVs could mediate the transfer of the drug-resistant phenotype, VSF from the NCC-HN120 CisR was added to NCC-HN120 WT cultures in the presence of cisplatin or paclitaxel. As predicted, NCC-HN120 WT cells treated with VSF collected from NCC-HN120 CisR cultures became more resistant to cytotoxic drug treatments, indicating that EVs containing high levels of TGFβ3 was sufficient to transfer the resistant phenotype. To further confirm that this effect was EV-mediated, sensitive cells were treated with the same NCC-HN120 CisR-VSF depleted of CTB- or AV-EVs. Drug response assays confirmed that EV depletion could abrogate the resistance-transfer, phenotype compared to intact/non-depleted NCC-HN120 CisR VSF. Similarly, VSF collected from SCC25$^{-TGF\beta3}$ was unable to induce resistance to cisplatin and paclitaxel in NCC-HN120 WT (**Figure 4C**). VSF-induced drug resistance was associated with increased SMAD2 phosphorylation with no effect on ERK phosphorylation, suggesting that the transfer of a resistance phenotype is associated with TGFβ downstream signaling (**Figure 4D**). Taken together, these results suggest that TGFβ3 present in EVs released by drug-resistant cells are able to activate SMAD2 phosphorylation to induce resistance in sensitive cells.

## Discussion

The clinical scenario in this study is not uncommon and remains an unmet need. The ability to predict treatment failures to CRT would re-direct HNSCC patients to appropriate curative therapies without delay. In fact, several groups have made attempts to identify factors that predict treatment response based on biological hypotheses and analyses of the primary tumor tissue itself. These include using fresh or archived tissue, and techniques such as miRNA expression, single protein biomarkers, complex multi-gene expression or multi-protein signatures (35-37). Extending these to crude plasma-based assays has met with little success to date.

The detection of circulating EVs could circumvent many challenges associated with plasma biomarker discovery. Circulating EV-based biomarkers is an emerging research area with great potential clinical relevance. Shao et al. (38) showed that the typing of proteins present in circulating microvesicles allows real-time monitoring of glioblastoma therapy response. One of the major technical issues in many such analyses is the reliability and reproducibility of capture techniques to isolate biologically relevant EVs, particularly the need to move beyond simple centrifugation-based isolation. We had previously shown that is it possible to isolate at least two distinct fractions of EVs in plasma according to CTB or AV ligands, which have a high specific binding affinity for ganglioside GM1 or phosphatidylserine present in the membrane of the respective EV fractions. This technique provides a highly specific method for the isolation of phospholipid membrane vesicles with minimal contamination of large non-vesicular biologic complexes or high abundant plasma proteins. Importantly, this method has been used to capture EVs from relatively small volumes of frozen biological fluids such as plasma and ascites to identify biomarkers in pre-eclampsia and ovarian cancer (30,39).

The importance of these findings is underscored by its clinical relevance. We were able to show, in the context of a controlled clinical trial, that TGFβ3 in plasma AV-EV fraction, served as biomarker for CRT response using a readily available ELISA kit. Our data suggest that in this specific set of patients with advanced HNSCC treated with organ-preservation protocol, high TGFβ3 levels in plasma AV-EVs was associated with disease progression, and with a dose-dependent likelihood of treatment failure on logistic regression models. While this is a relatively small cohort of 38 patients, the uniformity of within the confines of a phase II study contributes to the accuracy of these results, and supports the need for a future clinical trial where patients with high levels of TGFβ3 in AV-EVs are directed to more aggressive therapy or curative surgery rather than routine cisplatin-based CRT regimens.

TGFβ pathway has been shown to be important for EMT, stem cell states, and treatment resistance (40-42). Previous studies have implicated this pathway in chemo-resistance, specifically through TGFβ1 signaling via TGFβRII. In breast cancer, autocrine TGFβ signaling was shown to mediate paclitaxel resistance promoting cell survival via inhibition of apoptotic signaling (41). Furthermore, Oshimori et al. (42) observed that stem cells derived from squamous cell cancer respond to TGFβ1 treatment with increasing cisplatin resistance. In the latter context, TGFβ signaling results in the induction of p21, stabilization of NRF2, thereby markedly enhancing glutathione metabolism and diminishing the effectiveness of anticancer therapy. Several studies have demonstrated that TGFβ signaling is either dependent or independent of SMAD activation, where the major pathways are context-dependent or cell-type-specific (43). Moreover, Zhu et al. (44) demonstrated that chemotherapeutics agents (cisplatin and paclitaxel) could activate the TGFβ pathway by stimulating the phosphorylation of Smad2 and Smad3 in cervical and ovarian cancer cell lines. As such,

there is much interest in the role of TGFβ inhibitors as potential anti-metastatic agents or enhancers of cytotoxic treatment.

In this study, using commercially available lines and isogenic pairs of cisplatin-resistant/sensitive patient-derived lines, we also observed that TGFβ pathway plays a major role in HNSCC drug resistance. Specifically, TGFβ3 as being differentially expressed in drug-resistant HNSCC cell lines. Exogenous TGFβ3 induced resistance in drug-sensitive cell lines, while LY2109761 (a neutralizing TGFβRII antibody) sensitized drug-resistant cell lines. Incidentally, LY2109761 has been shown to sensitize a wide range of cancer cell lines (e.g. ovarian cancer, osteosarcoma) to cisplatin (45,46). We also found that HNSCC cell lines secrete TGFβ3 in extracellular vesicle, and the level of this protein in EVs was correlated with drug resistance. EV-enriched VSF from resistant cells conferred resistance when applied to sensitive cells. The depletion of CTB-/AV-EVs reduced the potency of VSF in conferring resistance. Additionally, EV-enriched VSF from TGFβ3 knockout cell line could not induce resistance on sensitive cells. VSF-mediated induction of drug resistance resulted in TGFβ3 downstream signaling in sensitive recipient cells with SMAD2 phosphorylation. TGFβ3 in the EVs were significantly higher than matched controls (plasma or cell culture medium), indicating that they are not non-specific contaminants. However, determining the location of TGFβ3 as being membrane-bound or within the lipid-bilayer of the EVs would be important in elucidating the molecular mechanism of action.

The role of EVs in transferring drug resistance is well documented by several mechanisms (11). EV-associated factors mediating drug resistance include DNMT1, miR-214, and miR-21-3p in ovarian cancer, lncRNA-ROR in hepatocellular carcinoma, miR-34a in prostate cancer, miR-100–5p in lung cancer, miR-21 in gastric cancer cells and in HNSCC (47-53). Other studies have also demonstrated that cancer-cell derived

EVs can induce TGFβ signaling via TGFβ/SMAD pathway activation and enhancing DNA repair activity through SMAD and downstream Lig4 expression, resulting the protection of epithelial cells from γ-radiation stress (54,55). Protein content profiling of EVs shed by sixty cell lines from the National Cancer Institute (NCI-60) found TGFβ3 secreted by melanoma, brain, breast, colon, kidney, lung, and ovarian cancers, but not HNSCC (56).

In summary, our results indicate that TGFβ3 transmitted through EVs plays a significant role in HNSCC resistance to cytotoxic therapy. High levels of this protein in plasma EVs is an independent predictor of disease progression in patients with locally advanced HNSCC treated with the chemoradiotherapy. We posit that the use of TGFβR inhibitors could be a novel sensitization approach in HNSCC patients with high TGFβ otherwise predicted to fail concurrent CRT. Important, these results demonstrate the potential of translating biological hypotheses involving extracellular vesicles into *bona fide*, clinically relevant biomarkers, using non-invasive monitoring.

**Funding**

This study was supported by grants from National Cancer Centre of Singapore Research Foundation (NMRC/CSA-INV/011/2016), Fundação de Amparo à Pesquisa do Estado de São Paulo – FAPESP (FAPESP, 2015/09182-0) and Exploit Technologies Pte and Biomedical Research Council (A*STAR; ETPL/12-R15GAP-0010). The sponsors had no role in the study design, collection and analysis, interpretation of the data, decision to publish, or writing the manuscript.

**Acknowledgements**

DMR-Jr acknowledges the support of the Coordenação de Aperfeiçoamento de Pessoal de Nível Superior (CAPES, 99999.007922/2014-00) and of the São Paulo Research Foundation (FAPESP, 2015/21420-3). ALV and ALC had a Conselho Nacional de Desenvolvimento Científico e Tecnológico – CNPq scholarship (300936/2015-0 and 561217/2010-6, respectively). NGI acknowledges the National Medical Research Council of Singapore Clinician Scientist Award (NMRC/CSA-INV/011/2016).

## Availability of data and materials

The datasets used and/or analyzed during the current study are available from the corresponding author on reasonable request.

## Authorship

DMRJR carried out the studies, data analyzes and manuscript draft. SST helped in the data analyzes. HSL developed the HNSCC resistant cells to cisplatin. LSV and ALC performed the clinical trial and collected the samples. MEM and CRNR carried out the CRISPR-Cas9 system production. LSK and DSWT helped to perform analyzes and the manuscript draft. NGI and ALV participated in study design, coordination and helped to draft the manuscript. All authors read and approved the final manuscript.

## Ethics approval and consent to participate

Written informed consent was obtained from all HNSCC patients. This study was approved by the institution ethics committees (CEP-UNIFESP: 1610/2016; CEP-HCBarretos: 231/2009).

## Consent for publication

Not applicable.

## Conflict of Interest

The authors declare that they have no competing interests.

# References

1. Jemal, A. et al. (2011) Global cancer statistics. CA Cancer J Clin, 61, 69-90.

2. Ferlay, J. et al. (2013) Cancer incidence and mortality patterns in Europe: estimates for 40 countries in 2012. Eur J Cancer, 49, 1374-1403.

3. Iyer, N.G. et al. (2015) Randomized trial comparing surgery and adjuvant radiotherapy versus concurrent chemoradiotherapy in patients with advanced, nonmetastatic squamous cell carcinoma of the head and neck: 10-year update and subset analysis. Cancer, 121, 1599-1607.

4. Viana, L.S. et al. (2016) Efficacy and safety of a cisplatin and paclitaxel induction regimen followed by chemoradiotherapy for patients with locally advanced head and neck squamous cell carcinoma. Head Neck, 38, e970-980.

5. Lococo, F. et al. (2015) Preliminary Evidence on the Diagnostic and Molecular Role of Circulating Soluble EGFR in Non-Small Cell Lung Cancer. Int J Mol Sci, 16(8), 19612-19630.

6. Yáñez-Mó, M. et al. (2015) Biological properties of extracellular vesicles and their physiological functions. J. Extracell. Vesicles, 4, 27066.

7. Colombo, M. et al. (2014) Biogenesis, secretion, and intercellular interactions of exosomes and other extracellular vesicles. Annu Rev Cell Dev Biol, 30, 255-289.

8. Tkach, M. et al. (2016) Communication by Extracellular Vesicles: Where We Are and Where We Need to Go. Cell, 164(6), 1226-1232.

9. Principe, S. et al. (2013) Tumor-derived exosomes and microvesicles in head and neck cancer: implications for tumor biology and biomarker discovery. Proteomics, 13, 1608-1623.

10. Plebanek, M.P. et al. (2017) Pre-metastatic cancer exosomes induce immune surveillance by patrolling monocytes at the metastatic niche. Nat Commun, 8(1), 1319-1331.

11. Samuel, P. et al. (2017) Mechanisms of Drug Resistance in Cancer: The Role of Extracellular Vesicles. Proteomics, 17, 1600375.

12. Gao, L. et al. (2018) Tumor-derived exosomes antagonize innate antiviral immunity. Nat Immunol, 19(3), 233-245.

13. Ramirez, M.I. et al. (2018) Technical challenges of working with extracellular vesicles. Nanoscale, 10(3), 881-906.

14. Ludwig, S. et al. (2017) Suppression of Lymphocyte Functions by Plasma Exosomes Correlates with Disease Activity in Patients with Head and Neck Cancer. Clin Cancer Res, 23, 4843-4854.

15. Whiteside, T.L. (2016) Exosomes and tumor-mediated immune suppression. J Clin Invest, 126, 1216-1223.

16. Rodrigues-Junior, D.M., et al. (2019) A preliminary investigation of circulating extracellular vesicles and biomarker discovery associated with treatment response in head and neck squamous cell carcinoma. BMC Cancer, 19, 373.

17. Cui, W. et al. (1996) TGFbeta1 inhibits the formation of benign skin tumors, but enhances progression to invasive spindle carcinomas in transgenic mice. Cell, 86, 531-542.

18. Lu, S.L. et al. (2006) Loss of transforming growth factor-beta type II receptor promotes metastatic head-and-neck squamous cell carcinoma. Genes Dev, 20, 1331-1342.

19. Bornstein, S. et al. (2009) Smad4 loss in mice causes spontaneous head and neck cancer with increased genomic instability and inflammation. J Clin Invest, 119, 3408-3419.

20. Lu, S.L. et al. (2004) Overexpression of transforming growth factor beta1 in head and neck epithelia results in inflammation, angiogenesis, and epithelial hyperproliferation. Cancer Res, 64, 4405-4410.

21. Feltl, D. et al. (2005) The dynamics of plasma transforming growth factor beta 1 (TGF-beta1) level during radiotherapy with or without simultaneous chemotherapy in advanced head and neck cancer. Oral Oncol, 41(2), 208-213.

22. Wunderlich, H. et al (1998) Increased transforming growth factor beta1 plasma level in patients with renal cell carcinoma: a tumor-specific marker?. Urol Int, 60(4), 205-207.

23. Kong, F. et al. (1999) Plasma transforming growth factor-beta1 level before radiotherapy correlates with long term outcome of patients with lung carcinoma. Cancer, 86(9), 1712-1719.

24. Maehara, Y. et al. (1999) Role of transforming growth factor-beta 1 in invasion and metastasis in gastric carcinoma. J Clin Oncol, 17(2), 607-614.

25. Tsushima, H. et al. (2001) Circulating transforming growth factor beta 1 as a predictor of liver metastasis after resection in colorectal cancer. Clin Cancer Res, 7(5), 1258-1262.

26. Song, B.C. et al. (2002) Transforming growth factor-beta1 as a useful serologic marker of small hepatocellular carcinoma. Cancer, 94(1), 175-180.

27. Ivanović, V. et al. (2006) Elevated plasma TGF-beta1 levels correlate with decreased survival of metastatic breast cancer patients. Clin Chim Acta, 371(1-2), 191-193.

28. Chia, S. et al. (2017) Phenotype-driven precision oncology as a guide for clinical decisions one patient at a time. Nat Commun, 8(1), 435-447.

29. Rasheed, S.A.K. et al. (2018) GNA13 expression promotes drug resistance and tumor-initiating phenotypes in squamous cell cancers. Oncogene, 37(10), 1340-1353.

30. Tan, K.H. et al. (2014) Plasma biomarker discovery in preeclampsia using a novel differential isolation technology for circulating extracellular vesicles. Am J Obstet Gynecol, 211(4), 380e1-e13.

31. Lai, R.C. et al. (2016) MSC secretes at least 3 EV types each with a unique permutation of membrane lipid, protein and RNA. J Extracell Vesicles, 5, 29828.

32. Rodrigues-Junior, D.M. et al. (2018) OIP5 Expression Sensitize Glioblastoma Cells to Lomustine Treatment. J Mol Neurosci, 66(3), 383-389.

33. Kapral, M. et al. (2008) Transforming growth factor beta isoforms (TGF-beta1, TGF-beta2, TGF-beta3) messenger RNA expression in laryngeal cancer. Am J Otolaryngol, 29(4), 233-237.

34. Ran, F.A. et al. (2013) Genome engineering using the CRISPR-Cas9 system. Nat Protoc, 8(11), 2281-2308.

35. Arantes, L.M. et al. (2017) Mir-21 as prognostic biomarker in head and neck squamous cell carcinoma patients undergoing an organ preservation protocol. Oncotarget, 8, 9911-9921.

36. Ong, C.J. et al. (2017) A three gene immunohistochemical panel serves as an adjunct to clinical staging of patients with head and neck cancer. Oncotarget, 8(45), 79556-79566.

37. Wang, W. et al. (2015) An eleven gene molecular signature for extra-capsular spread in oral squamous cell carcinoma serves as a prognosticator of outcome in patients without nodal metastases. Oral Oncol, 51, 355-362.

38. Shao, H. et al. (2012) Protein typing of circulating microvesicles allows real-time monitoring of glioblastoma therapy. Nat Med, 18(12), 1835-1840.

39. Reiner, A.T. et al. (2017) EV-Associated MMP9 in High-Grade Serous Ovarian Cancer Is Preferentially Localized to Annexin V-Binding EVs. Dis Markers, 2017, 9653194.

40. Heldin, C.H. (2009) Mechanism of TGF-beta signaling to growth arrest, apoptosis, and epithelial-mesenchymal transition. Curr Opin Cell Biol, 21(2), 166-176.

41. Bhola, N.E. et al. (2013) TGF-β inhibition enhances chemotherapy action against triple-negative breast cancer. J Clin Invest 123(3): 1348-1358.

42. Oshimori, N. et al. (2015) TGF-β promotes heterogeneity and drug resistance in squamous cell carcinoma. Cell, 160(5), 963-976.

43. Zhang, Y.E. (2009) Non-Smad pathways in TGF-beta signaling. Cell Res, 19, 128-139.

44. Zhu, H. et al. (2018) A Novel TGFβ Trap Blocks Chemotherapeutics-Induced TGFβ1 Signaling and Enhances Their Anticancer Activity in Gynecologic Cancers. Clin Cancer Res, 24(12), 2780-2793.

45. Ren, X.F. et al. (2015) LY2109761 inhibits metastasis and enhances chemosensitivity in osteosarcoma MG-63 cells. Eur Rev Med Pharmacol Sci, 19(7), 1182-1190.

46. Gao, Y. et al. (2015) LY2109761 enhances cisplatin antitumor activity in ovarian cancer cells. Int J Clin Exp Pathol, 8(5), 4923-4932.

47. Corcoran, C. et al. (2014) miR-34a is an intracellular and exosomal predictive biomarker for response to docetaxel with clinical relevance to prostate cancer progression. Prostate, 74(13), 1320-1334.

48. Takahashi, K. et al. (2014) Extracellular vesicle-mediated transfer of long non-coding RNA ROR modulates chemosensitivity in human hepatocellular cancer. FEBS Open Bio, 4, 458-467.

49. Pink, R.C. et al. (2015) The passenger strand, miR-21-3p, plays a role in mediating cisplatin resistance in ovarian cancer cells. Gynecol Oncol, 137(1), 143-151.

50. Cao, Y.L. et al. (2017) Exosomal DNMT1 mediates cisplatin resistance in ovarian cancer. Cell Biochem Funct, 35(6), 296-303.

51. Liu, T. et al. (2017) Exosomes containing miR-21 transfer the characteristic of cisplatin resistance by targeting PTEN and PDCD4 in oral squamous cell carcinoma. Acta Biochim Biophys Sin (Shanghai), 49(9), 808-816.

52. Qin, X. et al. (2017) Cisplatin-resistant lung cancer cell-derived exosomes increase cisplatin resistance of recipient cells in exosomal miR-100-5p-dependent manner. Int J Nanomedicine, 12, 3721-3733.

53. Zhang, J. et al. (2017) Curcumin suppresses cisplatin resistance development partly via modulating extracellular vesicle-mediated transfer of MEG3 and miR-214 in ovarian cancer. Cancer Chemother Pharmacol, 79(3), 479-487.

54. Gu, J. et al. Gastric cancer exosomes trigger differentiation of umbilical cord derived mesenchymal stem cells to carcinoma-associated fibroblasts through TGF-β/Smad pathway. PLoS One, 7(12), e52465.

55. Lee, J. et al. (2016) TGF-β1 accelerates the DNA damage response in epithelial cells via Smad signaling. Biochem Biophys Res Commun, 476(4), 420-425.

56. Hurwitz, S.N. et al. (2016) Proteomic profiling of NCI-60 extracellular vesicles uncovers common protein cargo and cancer type-specific biomarkers. Oncotarget, 7(52), 86999-87015.

## Legends: Figures and Tables

**Figure 1. TGFβ3 in plasma circulating EVs is a prognostic marker for HNSCC CRT.** TGFβ3 concentration was measured through ELISA-sandwich (LS-Bio) in EVs present in the plasma of HNSCC patients grouped according to their IC response (**A**) or CRT final response (**B**) (*$p < 0.0001$). (**C**) HNSCC patients progression-free survival in 4 years according to TGFβ3 concentration in AV-EVs ($p = 0.038$).

**Figure 2. HNSCC cell lines response to cisplatin treatment and expression of *TGFβ* isoforms. (A)** Assessment of $IC_{50}$ values for cisplatin treatment in NCC-HN120 WT and CisR, NCC-HN137 WT and CisR, FaDu, and SCC25 cell lines. RT-qPCR analysis was used to evaluate the relative expression level of *TGFβ1* (**B**), *TGFβ2* (**C**), and *TGFβ3* (**D**). All the relative expression levels were calculated using the $2^{-\Delta\Delta Ct}$ method. For all bar graphs, p-values denoted as: *$p < 0.05$, **$p < 0.01$, and ***$p < 0.0001$.

**Figure 3. The lack of TGFβ3 sensitizes HNSCC cell lines to cytotoxic therapies.** (**A**) The TGFβ3 knockout was performed with CRISPR-Cas9 system and verified by western blot. Knockout of TGFβ3 in SCC25 (**B** and **D**) and FaDu (**C** and **E**) induces sensitivity to cisplatin and paclitaxel, while exogenous TGFβ3 abrogated this sensitivity. The treatment with the inhibitor of TGFβ receptor (TGFβRi) sensitized CTRL HNSCC cells to cisplatin and paclitaxel treatments. HNSCC cell viability was quantified using CellTiter-Glo method (**B** and **C**) and apoptosis was assayed by Annexin V staining (**D** and **E**). Asterisks denote significance as determined by one-way ANOVA multiple comparisons followed by Bonferroni test (post-test); *$p<0.0001$, **$p<0.01$, ***$p<0.05$.

**Figure 4. TGFβ3 present in the EVs secreted by CisR HNSCC cells promotes resistance to cisplatin.** The relative TGFβ3 expression in CTB-EVs (**A**) and AV-EVs (**B**) shed by NCC-HN120 cell lines was measured through ELISA-sandwich (LS-Bio) and normalized by CD81 expression in the EVs. The significance was determined by Student's t-test (two-tailed) (**p*=0.0055 and **p*=0.0316, respectively). **(C)** NCC-HN120 WT cells were treated with VSF from NCC-HN120 CisR and SCC25$^{-TGFβ3}$ on the presence of cisplatin or paclitaxel. Asterisks denote significance as determined by one-way ANOVA, multiple comparisons followed by Bonferroni test (post-test) (**p* < 0.0001 and ** p = 0.0012). (**D**) Western blot assay showing activation of TGFβ pathway after co-treatment of NCC-HN120 WT with VSF from NCC-HN120 CisR cells and cisplatin. GAPDH was used as loading control.

**Table 1.** Correlation between TGFβ3 concentration in AV-EVs and CTB-EVs with clinical and pathological features. All p values were based on 2-tailed t-tests.

**Table 2.** Logistic regression analysis for factors predicting final CRT response.

**Supplementary Table 1.** gRNA sequences used in this study for CRISPR-Cas9 system.

**Supplementary Figure 1.** Receiver Operating Characteristic curves obtained for TGFβ3 in AV-EVs (AUC = 0.912) and CTB-EVs (AUC = 0.838), confidence interval: 95%.

**Supplementary Figure 2.** Curves of dose response for cisplatin treatment. Cell viability assays, based on CellTiter-Glo, were conducted to determine cell sensitivity to cisplatin in patient-derived primary cultures (NCC-HN120 and NCC-HN137) and commercial cell lines (FaDu and SCC25) of HNSCC. Each data point represents the average of three cell culture experiments per cell line per drug treatment.

**Supplementary Figure 3.** Characterization of EVs present in the Vesicular Secretome Fractions of NCC-HN120 cell lines. (**A**) The average size of EVs present in HNSCC VSFs was measured through ZetaView (Particle Metrix). The VSF were diluted 1,000X with filtered PBS (0.22μm) and analyzed by Nanoparticles Tracking Analysis software according to the manufacturer's protocol. The bars represent the average of three independent measurements. (**B**) Scanning electron microscopy (100,000x) of NCC-HN120 WT EVs that were isolated with CTB and AV. The VSF was incubated with biotinylated CTB, AV or without ligand and streptavidin coated polystyrene particles. The beads were then washed twice with filtered and suspended in 10x diluted with PBS. The beads without EVs interaction were used as negative control. The images were acquired in a FEI Quanta 250 FEG (ThermoFisher). (**C**) EVs were isolated with CTB and AV biotinylated ligands. After each isolated, the ligand-bound vesicles were removed with streptavidin-coated polystyrene particles, assayed for CD81 expression by ELISA and the relative expression level were normalized by the ratio of the number of total cells per total protein amount that was measured when the VSF was collected.

**Supplementary Figure 4.** Characterization of EVs present in the Vesicular Secretome Fractions of SCC25$^{-TGFβ3}$. (**A**) The size of nanoparticles was measured through NanoSight (Malvern). The VSF were diluted 1,000X with filtered PBS (0.22μm) and analyzed by Nanoparticles Tracking Analysis 2.3 software, according to the manufacturer's protocol. (**B**) The CD9 and CD81 expression present in SCC25$^{-TGFβ3}$ VSF was verified by western blot.

**Supplementary Table 2.** Clinical and histological characteristics of patients included in the study.

**TABLE 1.** Correlation between TGFβ3 concentration in AV-EVs and CTB-EVs with clinical and pathological features. All p values were based on 2-tailed t-tests.

| **Variable** | **Categories** | **Number of Cases** | **TGFβ3 in AV-EVs** | | p (2-tailed) | **TGFβ3 in CTB-EVs** | | p (2-tailed) |
|---|---|---|---|---|---|---|---|---|
| | | | Low | High | | Low | High | |
| | | | n (%) | n (%) | | n (%) | n (%) | |
| Age (years) | ≤ 60 | 27 | 16 (59.3) | 11 (40.7) | 1.00 | 15 (55.6) | 12 (44.4) | 1.00 |
| | > 60 | 11 | 7 (63.6) | 4 (36.4) | | 6 (54.5) | 5 (45.5) | |
| Gender | Male | 34 | 20 (58.8) | 14 (41.2) | 1.00 | 19 (55.9) | 15 (44.1) | 1.00 |
| | Female | 4 | 3 (75.0) | 1 (25.0) | | 2 (50.0) | 2 (50.0) | |
| Tobacco Consumption | Never | 2 | 1 (50.0) | 1 (50.0) | 0.948 | 0 (0.0) | 2 (100.0) | 0.235 |
| | Former | 8 | 5 (62.5) | 3 (37.5) | | 4 (50.0) | 4 (50.0) | |
| | Current | 28 | 17 (60.7) | 11 (39.3) | | 17 (60.7) | 11 (39.3) | |
| Primary site | Oral Cavity | 2 | 0 (0.0) | 2 (100.0) | 0.080 | 0 (0.0) | 2 (100.0) | 0.080 |
| | Oropharynx | 22 | 13 (59.1) | 9 (40.9) | | 11 (50.0) | 11 (50.0) | |
| | Hypopharynx | 5 | 5 (100.0) | 0 (0.0) | | 5 (100.0) | 0 (0.0) | |

| | | | | | | | | |
|---|---|---|---|---|---|---|---|---|
| | Larynx | 9 | 5 (55.6) | 4 (44.4) | | 5 (55.6) | 4 (44.4) | |
| HPV status | Positive (p16+) | 2 | 2 (100.0) | 0 (0.0) | 0.519 | 2 (100.0) | 0 (0.0) | 0.496 |
| | Negative (p16-) | 33 | 20 (60.6) | 13 (39.4) | | 18 (54.5) | 15 (45.5) | |
| Resectability status | Resectable | 24 | 16 (66.7) | 8 (33.3) | 0.492 | 15 (62.5) | 9 (37.5) | 0.318 |
| | Unresectable | 14 | 7 (50.0) | 7 (50.0) | | 6 (42.9) | 8 (57.1) | |
| Stage | III | 12 | 7 (58.3) | 5 (41.7) | 1.00 | 6 (50.0) | 6 (50.0) | 0.734 |
| | IV | 26 | 16 (61.5) | 10 (38.5) | | 15 (57.7) | 11 (42.3) | |
| CRT Response | CR | 22 | 17 (77.3) | 5 (22.7) | 0.012 | 15 (68.2) | 7 (31.8) | 0.157 |
| | NR | 13 | 4 (30.8) | 9 (69.2) | | 5 (38.5) | 8 (61.5) | |

Abbreviations: CR, complete response; NR, non-responders patients. All p values were based on 2-tailed t-tests.

**TABLE 2.** Logistic regression analysis for factors predicting final CRT response.

| Characteristic | Adjusted OR* (95% CI) | p-value |
|---|---|---|
| **TGFβ3 Expression in AV-EVs** | | |
| *Low expression* | 1 (ref.) | **0.016** |
| *High expression* | 9.14 (1.50 – 55.50) | |
| **Tumor Resectability** | | **0.021** |
| *Resectable* | 1 (ref.) | |
| *Unresectable* | 8.67 (1.34 – 54.84) | |

Figure 1

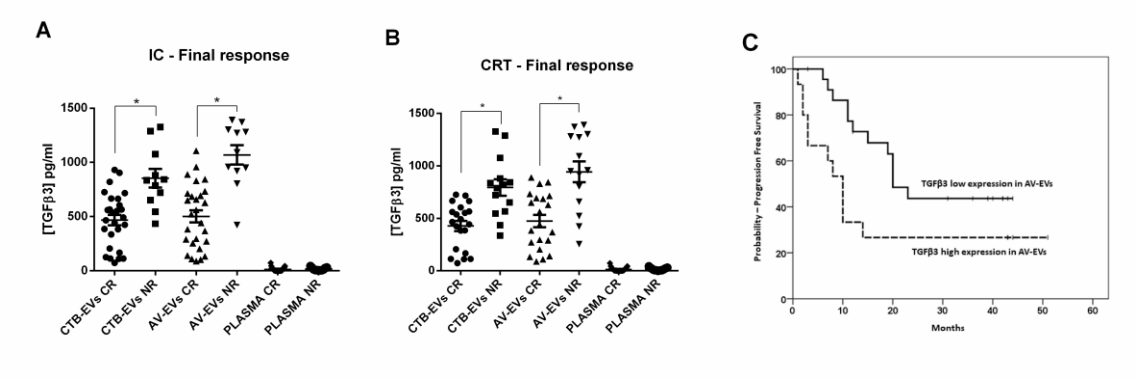

Figure 2

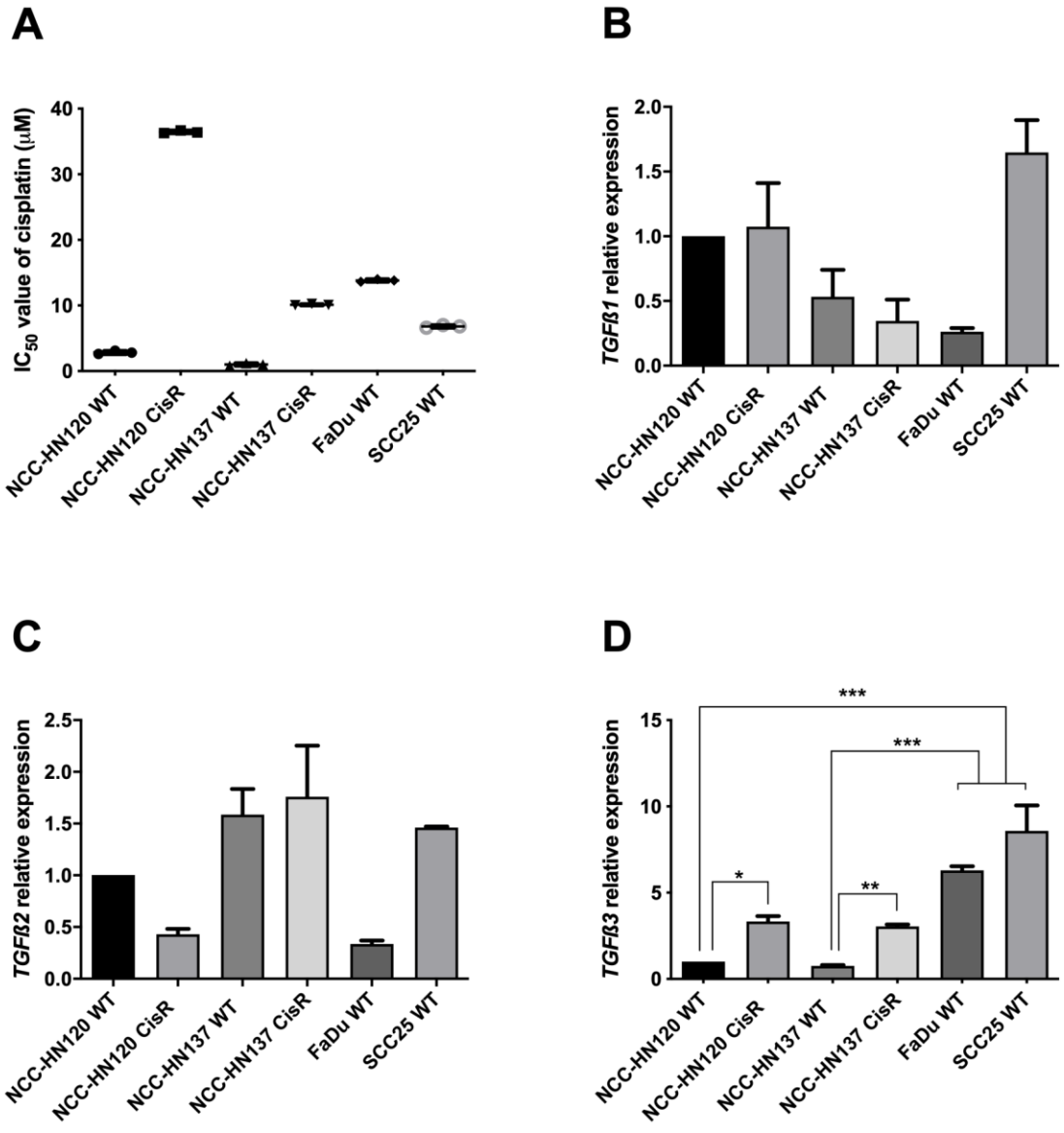

Figure 3

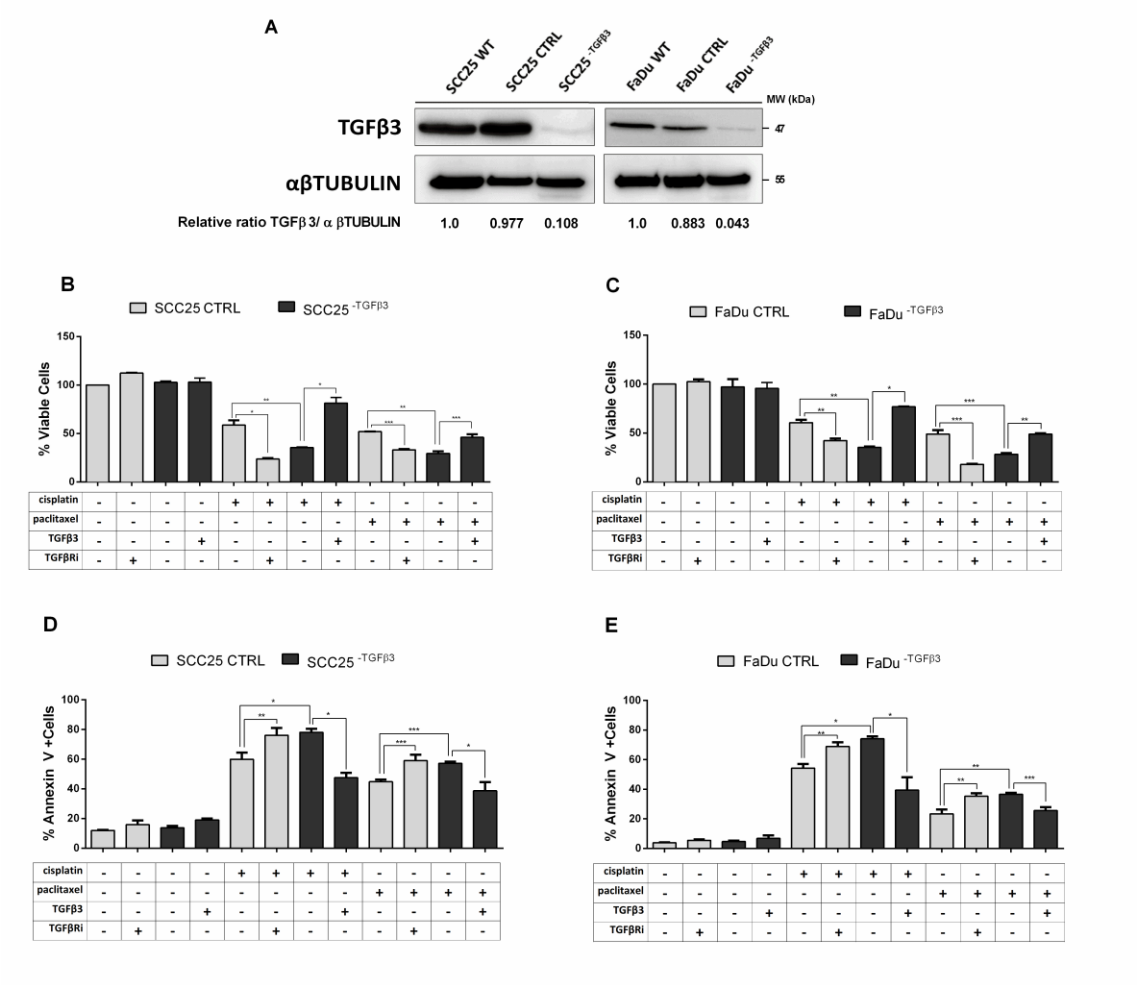

Figure 4